Circulation

High-Resolution Transcriptomic Profiling of the Heart During Chronic Stress Reveals Cellular Drivers of Cardiac Fibrosis and Hypertrophy

BACKGROUND: Cardiac fibrosis is a key antecedent to many types of cardiac dysfunction including heart failure. Physiological factors leading to cardiac fibrosis have been recognized for decades. However, the specific cellular and molecular mediators that drive cardiac fibrosis, and the relative effect of disparate cell populations on cardiac fibrosis, remain unclear.

METHODS: We developed a novel cardiac single-cell transcriptomic strategy to characterize the cardiac cellulome, the network of cells that forms the heart. This method was used to profile the cardiac cellular ecosystem in response to 2 weeks of continuous administration of angiotensin II, a profibrotic stimulus that drives pathological cardiac remodeling.

RESULTS: Our analysis provides a comprehensive map of the cardiac cellular landscape uncovering multiple cell populations that contribute to pathological remodeling of the extracellular matrix of the heart. Two phenotypically distinct fibroblast populations, Fibroblast-*Cilp* and Fibroblast-*Thbs4*, emerged after induction of tissue stress to promote fibrosis in the absence of smooth muscle actin–expressing myofibroblasts, a key profibrotic cell population. After angiotensin II treatment, Fibroblast-*Cilp* develops as the most abundant fibroblast subpopulation and the predominant fibrogenic cell type. Mapping intercellular communication networks within the heart, we identified key intercellular trophic relationships and shifts in cellular communication after angiotensin II treatment that promote the development of a profibrotic cellular microenvironment. Furthermore, the cellular responses to angiotensin II and the relative abundance of fibrogenic cells were sexually dimorphic.

CONCLUSIONS: These results offer a valuable resource for exploring the cardiac cellular landscape in health and after chronic cardiovascular stress. These data provide insights into the cellular and molecular mechanisms that promote pathological remodeling of the mammalian heart, highlighting early transcriptional changes that precede chronic cardiac fibrosis.

Micheal A. McLellan, BS*
Daniel A. Skelly, PhD*
Malathi S.I. Dona, PhD
Galen T. Squiers, BS
Gabriella E. Farrugia, BS
Taylah L. Gaynor, BS
Charles D. Cohen, BS
Raghav Pandey, PhD
Henry Diep, BS
Antony Vinh, PhD
Nadia A. Rosenthal, PhD
Alexander R. Pinto, PhD

*M.A. McLellan and Dr Skelly contributed equally.

Clinical Perspective

What Is New?

- Using novel methodologies and single-cell transcriptomics, this study maps the cellular landscape of the mouse heart and profiles intercellular communication in the context of angiotensin II–induced fibrosis.
- The study identifies 2 previously undescribed cardiac fibroblast populations that are key drivers of fibrosis; these do not correspond to smooth muscle actin–expressing myofibroblasts, which have been widely viewed as the primary drivers of cardiac fibrosis.
- The cardiac cellular landscape is sexually dimorphic at the cell abundance and gene expression level, including cellular responses to angiotensin II–induced tissue remodeling.

What Are the Clinical Implications?

- Identification of new drivers of fibrosis is pivotal for addressing multiple cardiac maladies in which fibrosis plays a prominent role.
- New fibrogenic cellular and molecular mediators identified in the study could be targeted to address development of cardiac fibrosis in women and men.
- Sexually dimorphic responses to physiological stress prompt consideration of sex-specific strategies to address the development of fibrosis in the heart and other cardiovascular tissues.

The mammalian heart is composed of a complex and heterogeneous network of cells. Although cardiomyocytes (CMs), the contractile cells of the heart, constitute the majority of cardiac cell mass, nonmyocytes far outnumber CMs.[1] Little is known about how the individual cellular components of the heart operate together as an integrated unit, how this cellular ecosystem is altered in the context of physiological stress, and how disparate cell populations may contribute to the functional decline that accompanies cardiac injury, aging, hypertension, or obesity. Moreover, although biological sex is recognized as an important variable in cardiovascular homeostasis and disease,[2] little is known about how biological sex affects transcriptional responses of distinct cardiac cell populations to chronic tissue stress.

To study the cardiac cellulome, the network of cells that forms the heart, in the context of chronic stress, we used an angiotensin II (AngII) cardiac hypertrophy model and applied a novel method for simultaneous transcriptional profiling of single CM nuclei and nonmyocyte cells. Our study revealed shared and distinct cellular pathways driving AngII-induced cardiac fibrosis.

Early fibrosis developed independently of smooth muscle actin–expressing (ACTA2+) myofibroblasts, a cell type conventionally recognized as a key mediator of cardiac fibrosis. This study also documents extensive sexual dimorphism in the gene expression profiles of cardiac cells, underscoring how biological sex influences responses to tissue stress. This work provides a valuable resource for cardiac cell biology research and offers important insights into the orchestrated cellular and molecular mechanisms that drive cardiac fibrosis and heart failure.

METHODS

For a detailed description of methods see Expanded Methods in the Data Supplement. All animal procedures were in accordance with institutional guidelines and approved by The Jackson Laboratory Institutional Animal Care and Use Committee or La Trobe University Animal Ethics Committee (AEC16-93). All sequencing data have been made publicly available at ArrayExpress and can be accessed by using accession number E-MTAB-8810.

Statistical Analysis

The methods used are described in detail in Expanded Methods in the Data Supplement and in figure legends (where appropriate). All P values considered statistically significant were ≤0.05.

RESULTS

Previous large-scale single-cell transcriptomic studies exploring cardiac cellular diversity have failed to profile key cardiac cell populations including CMs [3–6] because of a reliance on droplet-based sequencing approaches that are unable to process large cells. Moreover, extraction of CMs from rodent hearts typically requires retroaortic perfusion with proteases to liberate cells from the extracellular matrix (ECM); this is a relatively time-consuming process that has limited applicability for cell preparation in transcriptomic studies.[7]

To overcome these limitations, we developed a novel experimental framework to isolate and prepare all cardiac cells for single-cell RNA sequencing (scRNA-seq; Figure 1A). The goal of this approach was to profile all cardiac cell types with maximum possible throughput and accuracy, subject to limitations based on biological characteristics and current scRNA-seq instrumentation. Building on recent innovations in CM isolation,[8] we developed a perfusion-based tissue dissociation protocol that enables simultaneous isolation of cardiac cells from multiple hearts (see the Methods section; Figure 1A). To address the challenge of CM size, CMs were denuded of their cell bodies to liberate nuclei for droplet-based transcriptional profiling. As proof of concept, both CM nuclei and nonmyocyte nuclei were isolated independently and pooled for sequencing (Figure I in the Data

Figure 1. Isolation and analysis of the cardiac cellulome by scRNA-seq.
A, Schematic outline of the experimental procedure for the isolation and analysis of adult mouse cardiomyocytes and nonmyocytes by scRNA-seq. **B**, t-SNE projection of cardiac cells analyzed by scRNA-seq. Cells are colored by distinct cell populations as indicated. Note, the relative abundance of cell types displayed does not represent in vivo proportions (see Figure 1A and Expanded Methods in the Data Supplement). **C**, Heat map of relative expression of canonical cell markers in major cardiac cell populations. **D**, Top 5 distinct genes for each cell population, identified using an unsupervised approach. Dot color and size indicate the relative average expression level and the proportion of cells expressing the gene, respectively, within each cell population (also see Table I in the Data Supplement). DAPI indicates 4′,6-diamidino-2-phenylindole; DC, dendritic cells; ECs, endothelial cells; FACS, fluorescence-activated cell sorting; FSC-A, forward scatter area; lymph., lymphatic; NK, natural killer; and t-SNE, t-distributed stochastic neighbor embedding;

Supplement). Isolation of cells using this methodology yielded similar nonmyocyte cell proportions to protocols previously used,[4] although total cell yield and the number of extracted endothelial cells was lower (Figure II in the Data Supplement). Although isolation of nuclei overcame critical limitations related to CM size, for all further experimentation the nonmyocyte fraction was preserved as whole cells to provide access to total cellular RNA and to allow control of input cell proportions

for scRNA-seq by fluorescence-activated cell sorting using cell surface markers (Figure 1A).

After isolation of both CM nuclei and nonmyocyte cells, scRNA-seq was performed on a mixture of myocytes and nonmyocytes from untreated female and male hearts. We limited the relative number of endothelial cells and CM nuclei to minimize oversampling of these abundant cell populations at the expense of resolving less frequent cell types (Figure 1A). After the

clustering of 7474 cells derived from 2 mice of each sex (Figure 1B), examination of established marker genes and top enriched genes in each cell population (Figure 1C and 1D; Table I in the Data Supplement) revealed a wide array of cell types that were present in all samples (Figure III in the Data Supplement). These include fibroblasts (*Pdgfra, Col1a1*), pericytes (*Pdgfrb, Vtn*), smooth muscle cells (*Acta2, Myh11*), Schwann cells (*Plp1, Kcna1*), endothelial cells (*Pecam, Ly6c1*), macrophages (*Fcgr1, Csf1r*), and other immune cell populations (granulocytes, B cells, T cells, and natural killer cells). A subset of fibroblasts (Fibroblast-*Wif1*) showed distinct gene expression patterns including active Wnt signaling and specific expression of *Wif1*, in line with our previous report[4] and the findings of Farbehi et al.[5] Additional less well-characterized cell populations included CMs (*Ttn, Myh6*), epicardial cells (*Msln, Upk3b*), lymphatic endothelial cells (*Lyve1, Cldn5*), and endocardial cells (*Npr3, Cytl1*; Figure 1B through 1D).

In this study we examined pathological remodeling of the heart after 2 weeks of chronic AngII administration,

which corresponds to a relatively early stage of disease development (Figure 2A). An increase in heart mass and fibrotic area was noted in both female and male mice treated with AngII; however, hemodynamic changes and functional impairment were principally restricted to male mice that had a reduction of ejection fraction (Figure IV in the Data Supplement), in line with trends in human populations.[9] Histological analyses of hypertrophic mouse hearts showed a greater cross-sectional area and higher levels of fibrosis in both female and male hearts (Figure 2B and 2C; Figure V in the Data Supplement). Together these observations describe the pathological remodeling of the heart with AngII-induced pathological hypertrophy in both female and male contexts.

To examine cellular and molecular changes that accompany induction of fibrosis, we performed scRNA-seq on isolated myocytes and nonmyocytes in a total of 12 hearts from sham- and AngII-treated mice of both sexes. Combining these data with cells from the 4 untreated female and male hearts described earlier, we
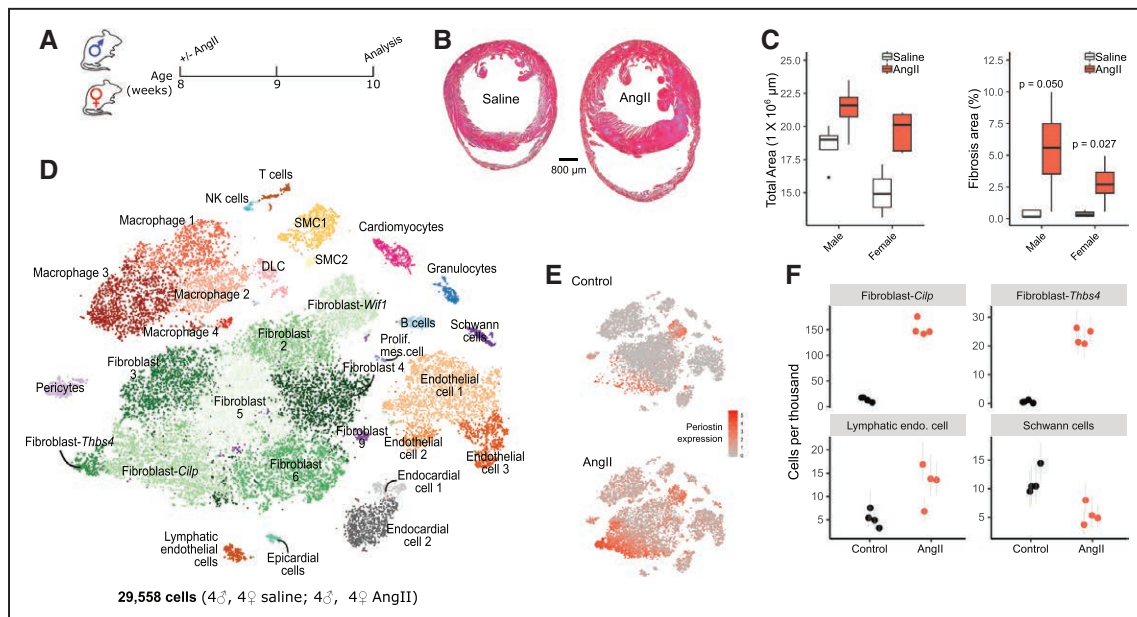

Figure 2. Histological and cellular changes in the heart after induction of cardiac fibrosis.
A, Experimental schema for AngII-mediated induction of cardiac fibrosis. Female and male mice were infused with AngII or saline (control) continuously for 2 weeks. **B**, Representative micrograph of trichrome-stained cardiac sections from mice infused with saline (**Left**) or AngII (**Right**). Example images shown are from female mice. **C**, Change in total cardiac area and cardiac fibrosis with and without induction of fibrosis in females and males (n=4–5 animals per group). Total cardiac area and fibrosis was quantified using high-resolution images of trichrome-stained midventricular sections as shown in **B** (also see Figure V in the Data Supplement). The entire cardiac section was used for measurements (see Expanded Methods in the Data Supplement). *P* values shown on plot are derived from the Wilcoxon rank sum test for differences between the groups. Whiskers of box and whisker plots represent highest and lowest value, except when a value is beyond the range of 1.5 interquartile. **D**, Fast Fourier transform–accelerated interpolation–based t-distributed stochastic neighbor (Flt-SNE) plot of cardiac cell clusters identified using single-cell transcriptional profiles of cells from mouse hearts with and without induction of fibrosis. In addition to the cell populations presented in **B**, this figure demonstrates more granular clustering of several major clusters (eg, fibroblasts, macrophages) and 2 additional populations (dendritic-like cells [DLC] and proliferating mesenchymal cells [Prolif. mes. cell]). **E**, Flt-SNE embedding projections of cardiac cells isolated from control (**Top**) and from fibrosis-induced (**Bottom**) mice. In the plot, reduced dimensionality space is divided into bins, and hexagons are colored according to mean Periostin (*Postn*) gene expression (red=high, gray=low) of cells in each bin to avoid distortion of patterns through overplotting. **F**, Change in proportion of selected cell populations in the single-cell RNA sequencing data set with and without fibrosis induction. Control mice include mice implanted with saline osmotic pumps (see the Methods section) and those that had not undergone any surgical interventions. Figure VI in the Data Supplement shows results for all cell populations. AngII indicates angiotensin II; NK, natural killer; and smc, smooth muscle cell.

obtained a total of 29 558 cells and performed clustering to identify a diverse array of cardiac cell types and subtypes (Figure 2D; Table II in the Data Supplement). Examination of cell abundances within this scRNA-seq data set revealed several cell populations that changed in relative prevalence in response to AngII (Figure 2E and 2F). Most notably, 2 fibroblast subpopulations that were not present at an appreciable number in unstressed hearts (Figure 2E and 2F; Figure VI in the Data Supplement) increased dramatically in hearts of mice treated with AngII and expressed high levels of periostin (Figure 2E). We refer to these cell populations as Fibroblast-*Cilp* and Fibroblast-*Thbs4*, reflecting markers that are highly expressed within these populations, with Fibroblast-*Cilp* being the largest cell population in this fibrosis data set. Subclustering fibroblasts did not significantly fragment fibroblast subpopulations further, whereas subclustering endothelial cells and dendritic-like cells yielded subpopulations that shifted in abundance with AngII treatment (Figure VII in the Data Supplement).

The limited input of specific cell populations for scRNA-seq analysis might restrict the detection of shifts in abundances of certain cell populations. To examine cell composition using an orthogonal method, we performed flow cytometric analysis of control and AngII-treated mouse hearts (Figure VIII in the Data Supplement). Macrophages significantly increased in abundance in males, compared with controls. However, there was no significant increase in fibroblasts detected by flow cytometry (Figure VIII in the Data Supplement), suggesting that Fibroblast-*Cilp* and Fibroblast-*Thbs4* represent a cell state arising primarily from resident fibroblasts rather than infiltration or proliferation of cells. Single-cell transcriptional profiling of cell cycle states revealed no significant increase in proliferation of fibroblast populations or in other cell types in response to AngII (Figure IX in the Data Supplement).

AngII treatment induced gene expression changes in all cardiac cell populations (Figure 3A; Figure X in the Data Supplement; Table III in the Data Supplement). Most notably, fibroblast populations up- or downregulated the greatest number of genes, with macrophage and endothelial cell subsets also exhibiting high responsiveness. Examination of the top 10 genes upregulated in response to AngII within each cell population revealed several patterns relevant to hypertrophy (Figure 3B; Table III in the Data Supplement). Among the top genes upregulated on AngII treatment were transcripts for *Cilp, Comp, Crlf1, Postn*, and *Thbs4*, some of which have been previously implicated in human heart failure.[10–12] These genes tend to be most highly expressed in only a few cell types but exhibit a significant increase in expression across many cell types under AngII treatment. Genes that were upregulated in clusters of cells or across a limited number

of cell populations included *Ms4a7* (macrophages) and *Gm13889* (pericytes and smooth muscle cells). Upregulated genes highly restricted to 1 cell type included *Ccl21a* (in lymphatic endothelial cells), and *Nppa* and *Nppb* (in CMs), which are well-established biomarkers of heart failure.[13] Gene ontology (GO) analysis of AngII-upregulated genes revealed that the top 3 enriched GO terms in most cardiac cell types contribute to remodeling of the cardiac ECM (Figure 3C; Table IV in the Data Supplement). Among the top genes downregulated in response to AngII, we observed a number of cell type–specific downregulated genes, in particular, in epicardial cells and multiple genes related to ATP synthesis and mitochondrial activity (Figure XIA in the Data Supplement; Table III in the Data Supplement). Downregulated genes also formed coherent gene programs, most notably in fibroblasts, related to protein translation and inflammation (Figure XIB in the Data Supplement; Table IV in the Data Supplement).

Cellular abundances of Fibroblast-*Cilp* and Fibroblast-*Thbs4* changed most dramatically on treatment with AngII (Figure 2F). To determine the effect of these cell populations on cardiac remodeling, we first compared differentially expressed genes between Fibroblast-*Cilp* and Fibroblast-*Thbs4* collectively with all other control cells within this data set, cardiac fibroblasts from control animals, and fibroblasts from AngII-treated animals (Figure 4A through 4C, respectively; Tables V and VI in the Data Supplement). Features common to basic fibroblast biology defined Fibroblast-*Cilp* and Fibroblast-*Thbs4* in comparison with all cardiac cells (eg, collagen and ECM organization). When contrasted with all fibroblasts from control animals or AngII-treated cohorts (Figure 4B and 4C, respectively), collagen-remodeling genes were the primary distinguishing features of Fibroblast-*Cilp* and Fibroblast-*Thbs4*. Comparison of Fibroblast-*Cilp* and Fibroblast-*Thbs4* also showed higher levels of ECM-remodeling genes in Fibroblast-*Cilp* than in Fibroblast-*Thbs4* (Figure 4D; Tables V and VI in the Data Supplement). Examination of total transcripts corresponding to ECM-remodeling genes suggests that Fibroblast-*Cilp* and Fibroblast-*Thbs4* are key contributors to ECM remodeling, with the Fibroblast-*Cilp* population contributing greater summed transcript abundance than all other fibroblast populations in AngII-treated mice (Figure 4E; Figure XII in the Data Supplement).

Fibroblast-*Cilp* and Fibroblast-*Thbs4* were also distinguished by the upregulation of genes such as *Thbs4, Fmod, Cthrc1*, and *Cilp*2 (Figure 4F; Table V in the Data Supplement). No genes were uniquely and highly expressed in Fibroblast-*Cilp* that were not also expressed in Fibroblast-*Thbs4*. THBS4+ cells in AngII-treated hearts were aggregated within foci and could also be identified as discrete cells (Figure 4Gi and 4Gii, respectively; Movie I in the Data Supplement; Figure XIII in the Data Supplement). An absence of THBS4+ cells surrounding
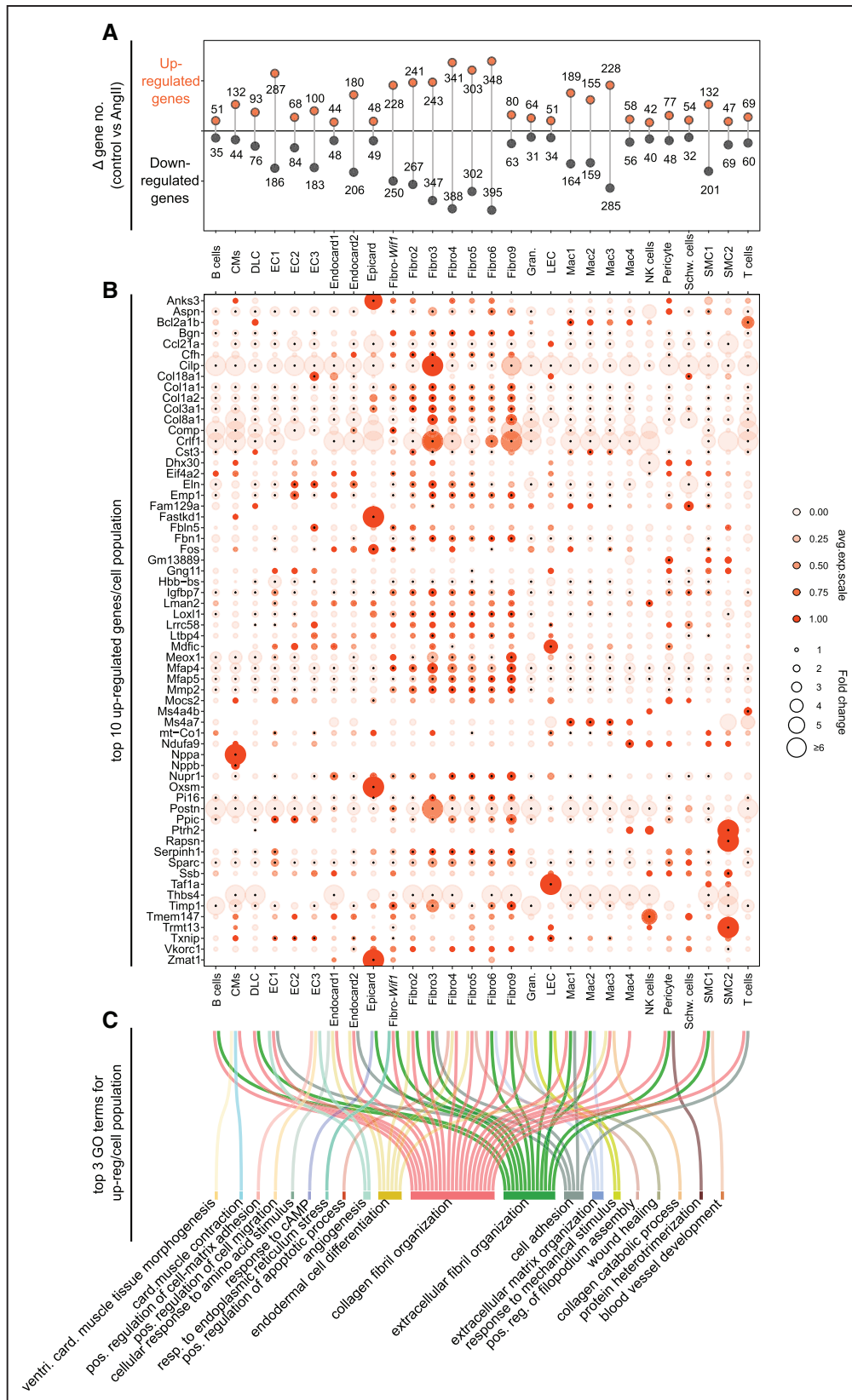
Figure 3. Gene expression changes in cardiac cell populations.
A, Lollipop plot summarizing number of up- and downregulated genes (uncorrected $P<0.01$) in AngII-treated mouse heart cells relative to control cohorts (see Table III in the Data Supplement). Note: We detected a statistically significant correlation between cell population size and number of differentially expressed genes discovered (Figure X in the Data Supplement). **B**, Dot plot summarizing the expression of genes identified as within the top 10 genes upregulated in response to AngII administration, for each cell type. Dot color and size are proportional to average expression within each cell cluster and fold increase in AngII cells relative to control cells, respectively. Black points at the centers of some dots indicate a significant difference in gene expression in response to AngII (uncorrected $P<0.01$). (*Continued*)

Figure 3 Continued. C, Sankey plot summarizing the top 3 GO terms for upregulated genes of each cell type (corrected *P*<0.05). Connections indicate GO terms associated with each cell type (see Table IV in the Data Supplement). Note: (1) many cell types upregulate genes that are associated with the same GO terms, consistent with a specific and choreographed response to a cardiac stressor; (2) not all cell types have 3 GO terms associated with their upregulated genes, (3) Fibroblast-*Cilp* and Fibroblast-*Thbs4* are excluded from this differential expression analysis because they are nearly absent in unstressed hearts. AngII indicates angiotensin II; card. cardiac; GO, gene ontology; pos. positive; reg., regulation; resp., response; and ventri., ventricular.

perivascular fibrotic lesions (Figure 4Giii) suggested that Fibroblast-*Thbs4* are principally involved in interstitial fibrosis. Last, in accordance with transcriptomic analyses, we confirmed that neither Fibroblast-*Cilp* nor Fibroblast-*Thbs4* corresponds to ACTA2⁺ myofibroblasts (Figure 4H and 4I). These findings suggest that Fibroblast-*Cilp* and Fibroblast-*Thbs4* may be transcriptionally similar to the matrifibrocyte, a specialized fibroblast state found in the mature scar after myocardial infarction.[14] Some expression of the matrifibrocyte markers *Comp*, *Sfrp2,* and *Wisp2*[6,14] was observed in Fibroblast-*Cilp*/*Thbs4* cells, although these genes were expressed at varying levels within the cluster, and cells with high expression of each marker did not colocalize. These genes are less specific for Fibroblast-*Cilp* and Fibroblast-*Thbs4* than *Cilp*, *Ddah1*, or *Thbs4* (Figure XIV in the Data Supplement).

To explore the origins of Fibroblast-*Cilp* and Fibroblast-*Thbs4*, we examined dynamic patterns of transcriptional activation and repression in detail in all fibroblasts using RNA velocity.[15,16] This analysis suggested that the Fibroblast-*Thbs4* population predominantly arises from Fibroblast-*Cilp*, whereas Fibroblast-*Cilp* has broader origins from Fibro5 and Fibro6 (Figure 5A). Use of 2 independent pseudo–time-based methods yielded results that were also concordant with these conclusions (Figure XV in the Data Supplement). Some transcripts expressed in both Fibroblast-*Cilp* and Fibroblast-*Thbs4*, such as *Cilp* and *Postn*, showed gradients in velocity across Fibroblast-*Cilp* into Fibroblast-*Thbs4* (Figure 5B and 5C), suggesting that Fibroblast-*Thbs4* cells represent a cell state characterized by transcriptional activation of a unique set of genes.

To determine the effect of AngII treatment on cardiac intercellular signaling, we mapped ligands and cognate receptors expressed by various cell populations (Figure 6; Table VII in the Data Supplement). As previously reported,[4] a similar analysis revealed extensive intercellular communication in unstressed hearts. Signaling by fibroblasts, along with macrophages, represented key features of the interstitial cardiac niche at baseline (Figure 6A; Figure XVI in the Data Supplement). Dendritic-like cells, epicardial cells, and endocardial cells were also significant populations forming extensive potential signaling networks within a diverse array of cell types (Figure 6A; Figure XVI in the Data Supplement). In contrast, consistent with previous analyses,[4] patrolling cell populations, granulocytes, natural killer cells, and lymphocytes, were among the least interactive cell

populations. Few interactions observed for CMs may be attributable to a lower number of genes and reads in this cell population attributable to transcriptional profiling of nuclei rather than whole cells.

Examination of factors essential for supporting specific cell populations points to important trophic intercellular interactions (Figure 6B). In addition to previously reported expression patterns for *Igf1*, *Il34*, *Ngf*, and *Ntf3* (Figure 6B),[4] epicardial cells were identified as the most highly enriched for *Csf1* transcripts, required for macrophage vitality, whereas CMs were the primary producers of *Vegfa* that supports endothelial cell growth (Figure 6B). Although the role of the epicardium in supporting macrophage trafficking in fetal development has been previously established,[17] this result suggests that epicardial cells are the most macrophage-trophic cell population by *Csf1*/*Csf1r* signaling (Figure 6B). The spatial distribution of macrophage subsets relative to the epicardium is distinct (Figure 6C), and further accentuated in older animals,[18] underscoring the epicardium and subepicardial space as a macrophage-trophic environment.

Cell–cell signaling in response to AngII-induced hypertrophy was increased in all cell types studied, with fibroblasts increasing the greatest number of connections (Figure 6D; Table VIII in the Data Supplement). GO enrichment analysis of upregulated connections between cell types revealed that the most frequently increased ligands involved cellular response to amino acid stimulus and collagen fibril organization (Figure 6E; Table IX in the Data Supplement); upregulated receptors included those interacting with ECM (Figure 6F; Table IX in the Data Supplement). Ligands involved in angiogenesis were upregulated in multiple cell types, whereas endothelial cells upregulated cognate receptors (Figure 6F; Table IX in the Data Supplement). Together these analyses suggest a concerted effort by multiple cell types in the cardiac cellulome to alter the cardiac niche and promote ECM remodeling.

Conversely, GO terms related to downregulated ligands suggests dampening of inflammation in the cardiac microenvironment (Figure XVII in the Data Supplement; Table IX in the Data Supplement), with almost all enriched GO terms related to inflammation or leukocyte/monocyte trafficking. It is intriguing that other GO terms enriched within downregulated ligands and receptors were associated with angiogenesis, suggesting that the up- and downregulation of receptors within
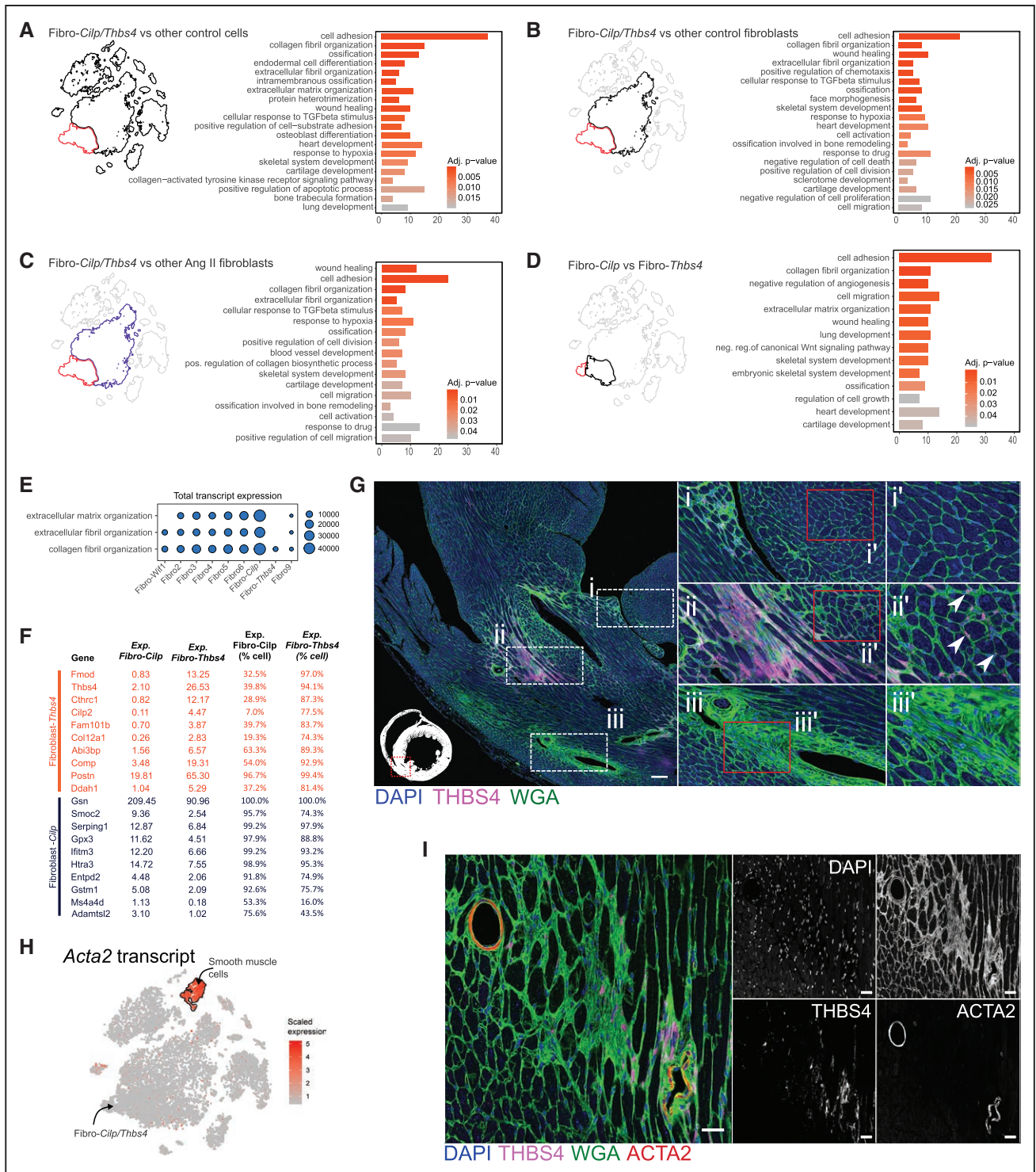
Figure 4. Distinguishing features of fibrosis-associated fibroblasts.
A, GO terms enriched in a set of genes derived from comparing gene expression differences between Fibroblast-*Cilp* and Fibroblast-*Thbs4* vs all other control cells. *x* axis indicates the number of genes mapped to each GO term, and color indicates the adjusted *P* value from GO enrichment analysis. Outline of Flt-SNE projection shown on Figure 2D, Left, indicates Fibroblast-*Cilp* and Fibroblast-*Thbs4* population (red) being compared with other cells (black; see Tables V and VI in the Data Supplement). **B**, Presentation of GO terms as in **A**, but associated with a comparison of Fibroblast-*Cilp* and Fibroblast-*Thbs4* vs fibroblasts from control mice. **C**, Presentation of GO terms as in **A**, but associated with a comparison of Fibroblast-*Cilp* and Fibroblast-*Thbs4* vs fibroblasts from AngII-treated mice. Purple Flt-SNE outline indicates AngII-fibroblasts being compared with Fibroblast-*Cilp* and Fibroblast-*Thbs4*. **D**, Presentation of GO terms as in **A**, but associated with a comparison of Fibroblast-*Cilp* to Fibroblast-*Thbs4*. **E**, Dot plot showing expression of fibroblast genes classified within the GO categories shown on *y* axis. Circle size represents the sum of transcripts for genes corresponding to each GO term within each cell population. See Figure XII in the Data Supplement for transcript levels of all cell types. **F**, Top 10 genes enriched for specific expression in either Fibroblast-*Cilp* (dark blue) or Fibroblast-*Thbs4* (orange) cell populations. Columns show average expression in each cell population expressed as either normalized read counts (in units of unique molecular identifiers per 10 000; columns 2–3) or percentage of cells with nonzero expression of the gene (columns 4–5). (*Continued*)

Figure 4 Continued. G, Micrograph showing AngII-treated mouse heart section stained with anti-THBS4 antibody, wheat-germ agglutinin (WGA; to identify cell boundaries and fibrosis), and DAPI (nuclei). Figure **insets** indicate regions without fibrosis (i and i′); dense THBS4+ fibrosis (ii) and perivascular fibrosis without THBS4 staining (iii and iii′). Region with discrete THBS4+ cells is also shown (ii′). Scale bar, 100 µm. Comparable staining was performed on >4 AngII-treated mouse hearts. See Figure XIII in the Data Supplement for control micrographs. **H**, Flt-SNE plot with cells colored according to *Acta2* transcript abundance (red=high, gray=low). Red outline indicates Fibroblast-*Cilp* and Fibroblast-*Thbs4* population. **I**, Micrograph labeled as in **F**, however with additional marker for ACTA2. Monochromatic images show intensity levels of individual fluorescence channels. Scale bar, 25 µm. Comparable staining was performed on >3 AngII-treated mouse hearts. ACTA2 indicates smooth muscle actin–expressing; Adj., adjusted; AngII, angiotensin II; DAPI, 4′,6-diamidino-2-phenylindole; Flt-SNE, fast Fourier transform–accelerated interpolation–based *t*-distributed stochastic neighbor embedding; GO, gene ontology; TGFbeta, transforming growth factor beta; and THBS4, thrombospondin 4.

endothelial cells may reflect changes in cellular phenotype and shifts in sensitivity to angiotrophic cues.

Analysis of hemodynamic and cardiac functional parameters, and quantification of tissue fibrosis, as well, suggested extensive sexual dimorphism in the development of pathological remodeling in response to AngII. Many upregulated genes are modulated by estradiol (Figure XVIII in the Data Supplement), and sexually dimorphic differences in cardiac cellularity after AngII treatment were detected by flow cytometry (Figure VIII in the Data Supplement). Moreover, fibrosis developed at specific anatomic loci to varying degrees in a sex-dependent manner (Figure 7A).

To explore sex-specific gene expression patterns within specific populations of the cardiac cellulome, we isolated female and male cells from control and AngII-treated groups based on the expression of genes expected to differ between sexes (chromosome X and Y genes outside the pseudoautosomal region; Figure 7B; Figure XIX in the Data Supplement). Comparison of proportions of female and male cell populations in control and AngII-treated hearts revealed no differences in cell abundance, with the exception of the Fibroblast-*Thbs4* population, where we observed ≈2-fold higher abundance of these cells in females than in males (Figure 7C).

Comparison of sex-specific gene expression differences within cell populations from both control and AngII-treated hearts revealed highly sexually dimorphic gene expression in almost all cell populations, with the greatest level of sexually dimorphic gene expression occurring within fibroblast subpopulations 2 and 4 to 6 in control hearts, and fibroblast subpopulations 2 to 6 and Fibroblast-*Cilp* of AngII-treated mice (Figure 7D and 7E; Tables X and XI in the Data Supplement). This is in line with the high enrichment of sex hormone receptors expressed by these cells (Figure XX in the Data Supplement).

Sexual dimorphism in the expression of genes upregulated after AngII treatment (Figure 7E and 7F; Figures XXI and XXII in the Data Supplement; Table XI in the Data Supplement) was predominantly detected in fibroblast populations (with the exception of Fibroblast-*Wif1* and Fibroblast-*Thbs4*), with very few genes differentially regulated in other cell types (Figure 7E; Table XI in the Data Supplement). Dimorphisms in expression were less evident in genes downregulated after cardiac fibrosis (Figure XXIII in the Data Supplement). Examination

of genes with ≥2-fold difference between sexes in cells of control hearts revealed a heterogeneous collection of genes (Figure XXIVA in the Data Supplement; Table X in the Data Supplement). These included genes encoding proteins such as GNGT2, CAMLG, TDP1, and NEK7 whose orthologs have been previously identified as sexually dimorphic in human heart failure.[19] GO enrichment analysis of sexually dimorphic genes in control hearts showed an enrichment of genes corresponding to antigen processing in multiple female cell populations and protein folding, stress, and angiogenesis in multiple male cell types (Figure XXIVB in the Data Supplement). Consistent with sexually dimorphic regulation of the endothelium, flow cytometric analysis of endothelial cells showed greater numbers of endothelial cells in male mouse hearts (Figure XXV in the Data Supplement). Genes such as *Vegfa* were upregulated in male (but not female) CMs and Fibroblast-*Thbs4* populations from AngII-treated mice, further suggesting sexually dimorphic angiogenic stimulation (Figure 7E). Among genes upregulated or downregulated in either sex (Figure XXII in the Data Supplement), female hearts had an enrichment of ECM-remodeling genes among the upregulated genes in Fibro6 and Fibroblast-*Cilp*, whereas males showed upregulation of genes involved in protein folding or responses to endoplasmic reticulum stress (Figure 7E). We also observed upregulation of ECM-organizing genes in male Fibro6 cells that were distinct from those upregulated in female Fibro6 or Fibroblast-*Cilp* populations, underscoring a potential difference in the characteristics of ECM generated in the 2 sexes on tissue stress. GO enrichment analysis revealed no coherent biological themes shared among downregulated genes, principally in fibroblasts, whose expression was sexually dimorphic.

To determine whether Fibroblast-*Cilp* and Fibroblast-*Thbs4* populations are also present in the context of human pathological remodeling, we analyzed bulk cardiac RNA-seq data from 85 women and 172 men between the ages of 40 and 69 profiled by the Genotype-Tissue Expression Project. Expression of the *NPPB* transcript was examined to segregate humans without and with putative hypertrophy; this gene codes for the cardiac hypertrophy biomarker B-type natriuretic peptide. High *NPPB* expression was used as a rough proxy for potential hypertrophy, and samples with the highest (top 20%) *NPPB* expression (without regard to age
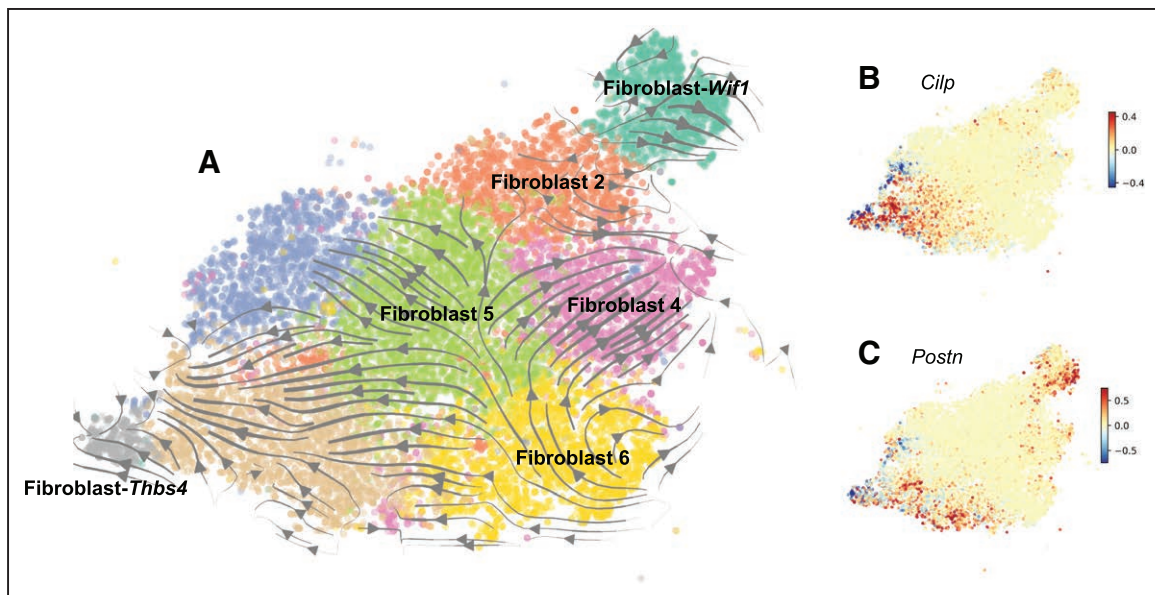
Figure 5. Shifts in fibroblast cell state in response to chronic stress imposed by AngII treatment.
A, Stream plot depicting patterns of RNA velocity in fibroblasts from mice administered AngII. Velocities were calculated using scVelo.[16] Clustering of fibroblasts and their placement in 2-dimensional space are identical to Figure 2D. RNA velocities are projected onto this Fourier transform–accelerated interpolation–based *t*-distributed stochastic neighbor embedding embedding for visualization purposes. Lines with arrows depict predominating changes in velocity and their associated directionality. **B**, Estimation of RNA velocity for *Cilp* in fibroblasts from AngII-treated mice. Relative velocities are colored according to scale on the right. **C**, As in **B**, but for *Postn*. AngII indicates angiotensin II.

or sex) were classified as putatively hypertrophic (Figure XXVIA in the Data Supplement). Expression of *POSTN*, *TGFB1*, and collagens was significantly elevated in all hypertrophy groups in comparison with corresponding no-hypertrophy controls (uncorrected *P*<1e-07 for all genes; Figure XXVIB in the Data Supplement) confirming that human hypertrophy cohorts also exhibit other markers of cardiac stress. Expression of *THBS4*, *DDAH1*, *FMOD*, *CTHRC1*, and *CILP,* 5 genes that are enriched in Fibroblast-*Cilp* and Fibroblast-*Thbs4,* was significantly increased in hypertrophic human hearts (1.4e-09 < *P* < 2e-03 for all genes, uncorrected; Figure XXVID in the Data Supplement). The overall concordance of these observations is striking because of the limitations of this underpowered statistical analysis, including imperfect status of *NPPB* transcript as a biomarker for heart failure, the inconsistency of human heart sample isolation, and age-dependent changes in the systemic milieu such as the onset of menopause. Nevertheless, our observations suggest that cells corresponding to Fibroblast-*Cilp* and Fibroblast-*Thbs4* may be present in the context of human cardiac stress.

DISCUSSION

Although a great deal of data exist concerning individual cellular components that contribute to cardiac dysfunction, less is known about how these components interact during concerted pathological responses to tissue stress. To clarify the roles of distinct heart cell populations in the context of chronic maladaptive cardiac stress responses leading to fibrosis, we developed a strategy enabling unbiased analysis of myocyte and nonmyocyte transcriptomes in parallel using scRNA-seq. This generated a high-resolution atlas of the cardiac cellulome with and without fibrosis. Virtually all cell types in the heart have detectable transcriptional responses to tissue stress, with most cells participating in remodeling of the ECM. Specifically, 2 activated fibroblast populations emerge in response to stress, presumably to remodel the extracellular environment by direct ECM deposition and paracrine regulation of the heart cell niche. The extensive sexual dimorphism of cell-specific gene expression in resting and maladaptive hearts implicates sex-specific mechanisms driving cardiac physiology and stress responses. Overall, this study provides insight into the cellular and molecular drivers of cardiac pathological remodeling and fibrosis.

As a resource for researchers, the extensive data set presented here comprises a deep and comprehensive map of the cardiac cellulome. These data were derived from 8 individual scRNA-seq libraries, with each library composed of female and male cells from a single animal of each sex. Cells from the 16 individual biological specimens can be isolated in silico to moderate effects of outliers and to examine the effect of biological sex on cardiac homeostasis and disease, which is an under-examined area in cardiac cell biology and physiology. [2,20]

Our analysis attained a detailed portrait of the intercellular circuitry supporting the heart cell network at
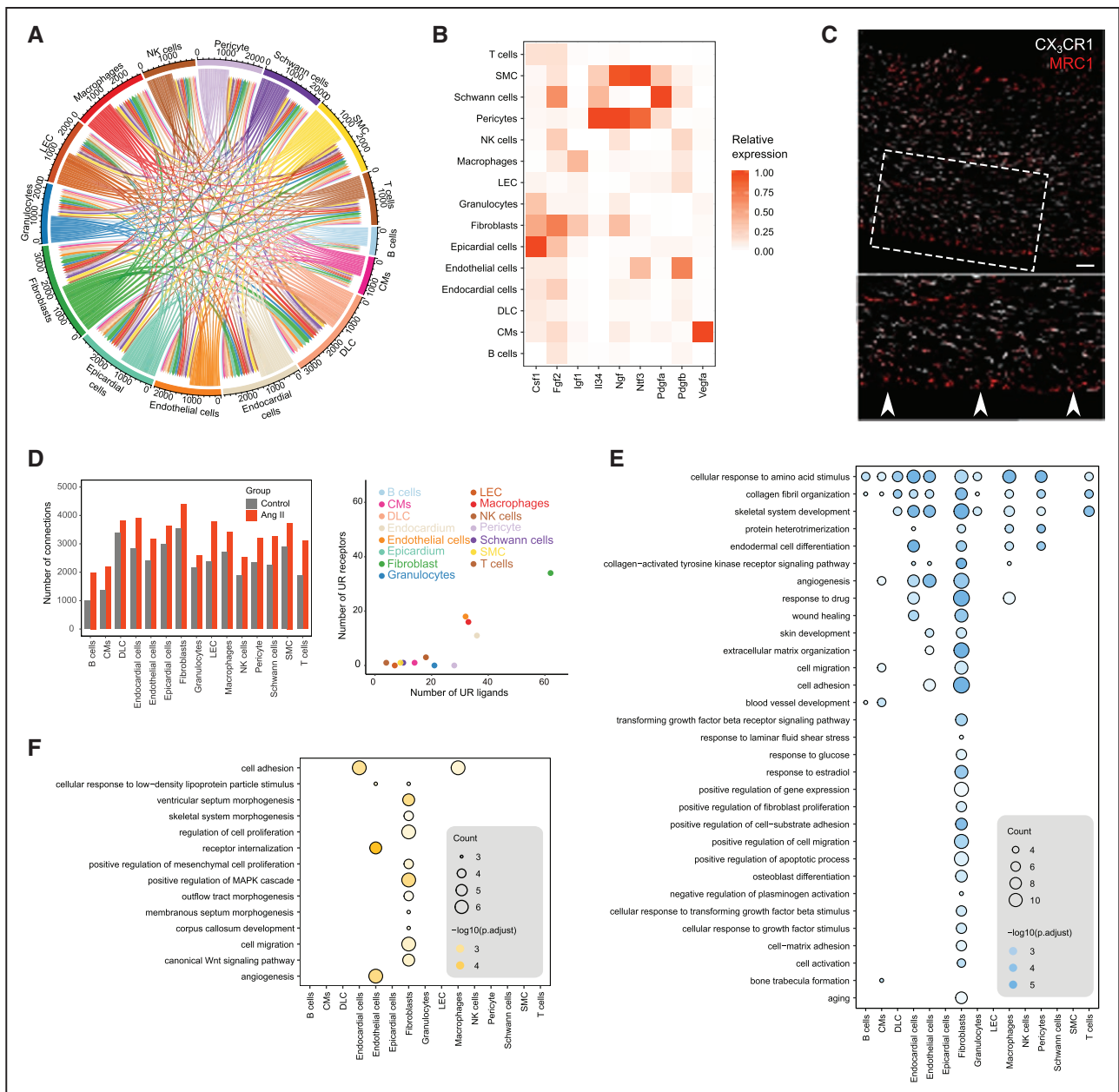
Figure 6. Intercellular connection network of the cardiac cellulome.
A, Chord plot summarizing interconnections between different cardiac cell types from hearts of control mice. Lines represent potential interconnections between cell types, with line thickness proportional to the number of ligand-receptor pairs expressed in the connected cell types and line color reflecting the cell population producing transcript coding for the ligand. See Expanded Methods section "Ligand-receptor intercellular communication network analysis" in the Data Supplement for more details. **B**, Relative expression of a selection of essential growth factors across major cardiac cell types. Gene expression is normalized to the expression level of the cell type with the greatest mean expression. **C**, Spatial distribution of MRC1+ and MRC1− macrophages relative to the epicardium in *Cx3cr1*$^{gfp/+}$ mouse hearts. Green fluorescent protein (white) labels both MRC1+ and MRC1− macrophages. Scale bar, 100 μm. **Inset** shows magnified view of the epicardium (indicated by white arrows). **D**, Number of receptor-ligand pairs potentially mediating cell–cell communication for each cell population with and without AngII treatment. Bar plot shows total number of connections (receiving and transmitted signals) made by each cell type without (gray bars) and with AngII treatment (orange bars; also see Table VII in the Data Supplement). Scatter plot summarizes number of upregulated receptors and ligands for each cell population (uncorrected *P*<0.01). Note: Dots corresponding to Schwann cells, epicardial cells, and B cells overlap because they have the same number of upregulated ligands and receptors (also see Table VIII in the Data Supplement). **E**, GO terms enriched in a set of genes that encode ligands upregulated after fibrosis induction. GO terms are ordered by their frequency of significant enrichment in different cardiac cell populations. **F**, GO terms enriched in a set of genes that encode receptors upregulated after fibrosis induction. GO terms are ordered by their frequency of significant enrichment in different cardiac cell populations (also see Table IX in the Data Supplement). AngII indicates angiotensin II; CM, cardiomyocyte; DLC, dendritic-like cell; GO, gene ontology; LEC, lymphatic endothelial cell; NK, natural killer; and SMC, smooth muscle cell.

homeostasis and in response to the induction of pathological hypertrophy. For example, this data set implicates epicardial cells as critically important for supporting

macrophage vitality and trafficking in the adult heart. Fibroblast-derived *Csf1* and mural cell–derived *Il34* are both growth factors that support macrophages that we
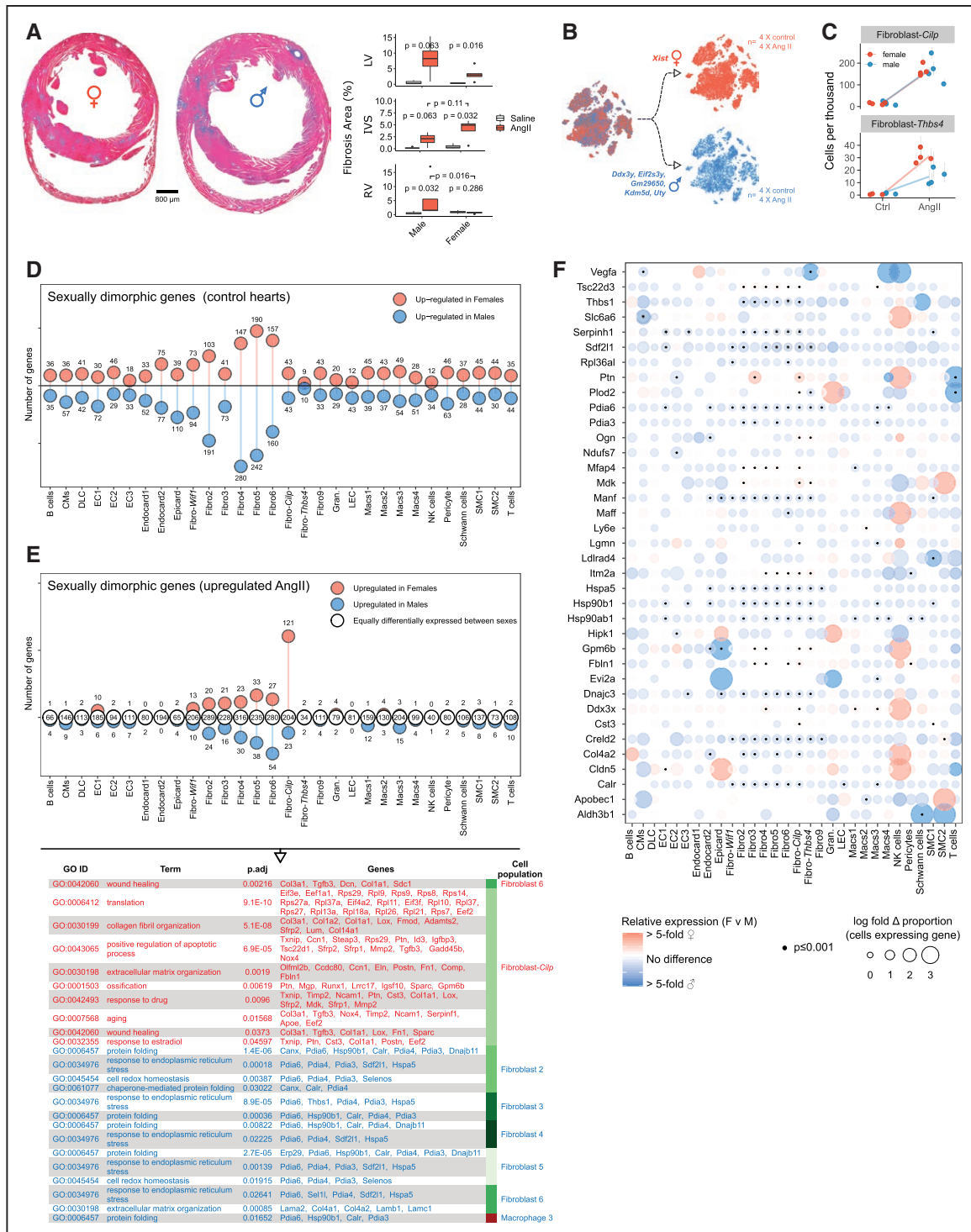
Figure 7. Sexual dimorphic remodeling and cellular responses.
A, Trichrome-stained sections from female and male hearts (**Left**, micrographs) and quantification of fibrosis (**Right**, boxplots). Plots summarize fibrosis in the left ventricles (LV), intraventricular septums (IVS), and right ventricles (RV) of male and female hearts (n=4–5 animals per group). Uncorrected *P* values determined using Wilcoxon rank sum test for differences between the groups. Whiskers of box-and-whisker plots represent highest and lowest value, except when a value is beyond the range of 1.5 interquartile. **B**, Illustration of the desegregation of female and male cells based on sex-specific gene expression. Cells are visualized as points in Flt-SNE space, identically to Figure 2D. As expected, female and male cells are each present within each cell cluster. **C**, Cellular abundances of Fibroblast-*Cilp* and Fibroblast-*Thbs4* populations in females and males with and without fibrosis induction. Light gray lines indicate binomial proportion confidence intervals and are calculated using the Jeffreys interval. Individual female and male mice are indicated by red and blue dots, respectively. The y axis shows cell abundance and regression lines derived separately from female and male samples (red and blue, respectively). **D**, Number of sexually dimorphic genes in cardiac cell types from hearts without (control) fibrosis induction (uncorrected *P*<0.01). Number of genes at significantly higher levels in females and males is indicated for each cell type by red and blue circles, respectively (see Table X in the Data Supplement). **E**, Sexually dimorphic gene expression of genes upregulated in cardiac cells after AngII treatment. See Methods section, Figure XXII in the Data Supplement, and Tables XI and XII in the Data Supplement for details. A summary of GO terms of genes upregulated in female cells (red text) or male cells (blue text) is shown in the table (below). Note: Consistent with a positive relationship between cell number and power to detect sexually dimorphic gene expression, we observed a statistically significant correlation between cell population size and the number *(Continued)*

Figure 7 Continued. of sexually dimorphic genes identified (Figure XXI in the Data Supplement). **F**, Dot plot summarizing the expression of genes changing in a sexually dimorphic manner in response to AngII. Plot shows genes that are upregulated after AngII treatment and differentially expressed between corresponding female and male cells (uncorrected $P<0.001$). Dot color and size are proportional to the relative expression and relative proportion of cells expressing the gene compared between females and males. AngII indicates angiotensin II; CM, cardiomyocyte; DLC, dendritic-like cell; EC, endothelial cell; F, female; GO, gene ontology; LEC, lymphatic endothelial cell; M, male; NK, natural killer; and SMC, smooth muscle cell.

previously detected in the heart[4]; however, the current analysis found that epicardial cells are the most macrophage-trophic cardiac cell population as a result of their high production of *Csf1*. Moreover, we identified distinct spatial distributions of macrophage subsets at the epicardium, suggesting additional unidentified regulation of macrophage positioning and trafficking. These results further support the important role of epicardial cells in macrophage homeostasis, in accordance with previous studies demonstrating the role of the epicardium in macrophage colonization of the heart.[17] Also notable was the identification of CMs as the principal producers of *Vegfa,* which is a dominant endothelial and angiogenesis growth factor. Although we have not examined the precise isoforms of *Vegfa* expressed by cardiac cells, our analysis indicates that the cell type perhaps most dependent on tissue perfusion is the key driver of vascular innervation of the heart.

Examination of ligand genes upregulated after induction of hypertrophy suggests the cardiac cellular niche is altered to support ECM remodeling and angiogenesis. This corresponded with upregulation of receptor genes mediating cell adhesion in a wide variety of cells, whereas angiogenesis-related receptors were upregulated in endothelial cells. GO enrichment analysis of all genes upregulated after induction of fibrosis indicated that a primary response of most cell types is the activation of genes involved in ECM remodeling. However, Fibroblast-*Cilp* and Fibroblast-*Thbs4* appear to be the most fibrogenic cell populations based on the expression of transcripts related to ECM remodeling GO terms. Their fibrogenic phenotype is further accentuated in comparison with other fibroblast populations from AngII-treated mice that extensively activate ECM remodeling and collagen genes.

Fibroblast-*Cilp* and Fibroblast-*Thbs4* do not constitute classically defined myofibroblast populations, widely accepted as the main protagonists driving fibrosis.[21] Recent scRNA-seq studies examining myocardial infarction have readily detected ACTA2+ myofibroblasts [5,6,22,23]. The experimental conditions of these reports represent examples of tissue trauma where myofibroblast activation may mediate wound healing. In contrast, *Acta2* transcript was not detected in Fibroblast-*Cilp* or in Fibroblast-*Thbs4* above background transcriptomic levels, or at the protein level by histology. A lack of smooth muscle α-actin would be consistent with the absence of a need for structural support in a necrotic area. Fibrosis without myofibroblast conversion has been reported in a model of diabetic cardiomyopathy,[24] and this fibrosis data set underscores that accumulation

of extensive fibrosis in the heart is not dependent on ACTA2+ myofibroblasts.

Fibroblast-*Cilp* and Fibroblast-*Thbs4* exhibit a closer resemblance to matrifibrocytes that reside in a mature scar after myocardial infarction.[14] Although expression of key matrifibrocyte marker genes, *Comp, Sfrp2,* or *Wisp2*, was not highly enriched in cells defined as Fibroblast-*Cilp* and Fibroblast-*Thbs4* in this study, the functional inferences made of these cell populations are comparable. Therefore, cells analogous to Fibroblast-*Cilp* and Fibroblast-*Thbs4* may promote fibrosis in multiple cardiac stress contexts.

Extending on these findings, we examined expression of transcriptional signatures resembling Fibroblast-*Cilp* and Fibroblast-*Thbs4* in the human context. Specifically, using human heart bulk RNA-seq data from normal and putatively hypertrophic cardiac samples, we found that genes with restricted expression to Fibroblast-*Cilp* and Fibroblast-*Thbs4* appear to be upregulated in hypertrophy and correlate with the cardiac stress marker NPPB. This finding suggests that future studies targeting Fibroblast-*Cilp* and Fibroblast-*Thbs4*, or genes specifically activated within these cell subsets, may yield therapeutically relevant outcomes for addressing human disease.

Analysis of downregulated genes indicates that a key feature of fibrosis induction is dampening of inflammation and leukocyte infiltration. Downregulated genes included CC chemokine ligands, which are key monocyte chemoattractants. Although AngII infusion caused an increase in macrophage abundance, observed by flow cytometry, this was not accompanied by significant increases in proinflammatory mediators. This suggests that the cardiac cellulome functions to dampen inflammation to regulate inflammatory responses. Furthermore, we found that mitochondrial bioenergetics are subdued in many cell types, in particular, in endothelial cells and macrophages, in accordance with the association between mitochondrial activity and heart failure.

The current study also identified numerous cell type–specific genes that were robustly upregulated in hypertrophy (such as *Rapsn* in smooth muscle cells or *Fastkd1* in epicardial cells) with unknown implications for cardiac pathology. Similar relationships were observed among downregulated genes (eg, *Thap8* in macrophages or *Has1* in the epicardium). These genes constitute appealing subjects for further research to explore their expression in further detail and their validity as potential therapeutic targets.

Analysis of the abundance of Fibroblast-*Cilp* and Fibroblast-*Thbs4* cell populations suggests sex differences in cellular abundance (Figure 7C), which is of particular

interest in light of known sexual dimorphisms in cardiac stiffness.[25] Indeed, analysis of cardiac fibrosis in AngII-treated mice revealed differences in fibrotic area in addition to the distribution of fibrotic loci. Females were characterized by less fibrosis in the left ventricle wall and the absence of fibrosis in the right ventricle walls, and less perivascular fibrosis, as well. In contrast, greater fibrosis accumulated in the female interventricular septum than in males, although a functional decline was only observed in males.

In both the unstressed and stressed contexts, sexual dimorphisms were observed in cardiac gene expression across almost all cell types, with particularly robust differences in fibroblasts that are the major sex hormone receptor–expressing cells in the heart. In the context of cardiac fibrosis, female and male cardiac fibroblasts regulated distinct sets of genes that are associated with ECM remodeling, suggesting that cardiac ECM quality is biologically distinct in the 2 sexes.

A key sexually dimorphic characteristic is the upregulation of genes related to unfolded protein responses (UPR) and endoplasmic reticulum stress in multiple male cell populations. UPRs may explain, at least in part, 2 sexually dimorphic features observed in this fibrosis data set. First, an increase in UPR may contribute to the increased fibrosis observed in male hearts (Figure 7A). Endoplasmic reticulum stress is observed in multiple models of tissue fibrosis including models of maladaptive cardiac remodeling,[26] and attenuation of UPR inhibits fibrosis.[27–29] Second, UPR may contribute to downregulation of translation-related genes in males. UPR may elicit this by multiple means including IRE1-mediated translational control of the transcription factor *Xbp1*, and regulation of multiple genes including *eukaryotic initiation factor* (*Eif*) genes and others involved in protein translation.[26] Incidentally, *Xbp1* is upregulated in multiple male cardiac cell types and is associated with tissue fibrosis in the heart and elsewhere.[30,31]

In addition to the link between protein translation and UPR, translation is also supported by estrogens in several species and in both neoplastic and non-neoplastic tissues.[32–34] In tumor cells, inhibition of estrogen receptor α induces UPR.[32] Moreover, estrogen has been recently shown to regulate *Eif* genes to promote protein synthesis.[35] Many *Eif* genes are upregulated after AngII infusion across multiple female cell populations in addition to many ribosomal protein genes. Together, these observations suggest that female cells are better primed for protein synthesis, and avoidance of tissue fibrosis and maladaptive remodeling, as well.

Conversely, the enrichment of genes implicated in angiogenesis was observed in multiple male cardiac cell populations including Fibro 2 and Fibro 6 in unstressed mice. Accordingly, increased numbers of endothelial cells were found in male hearts than in female hearts. In addition, significantly higher *Vegfa* expression was detected in male CMs and Fibroblast-*Thbs4* cells after fibrosis induction. Although estrogen has been reported to enhance angiogenesis in a range of contexts,[36] more recent research suggests that loss of estrogen receptor promotes angiogenesis.[37] Moreover, testosterone induces angiogenesis in a sex-dependent manner, further underscoring the importance of the hormonal milieu.[38] Last, UPR is also strongly linked to upregulation of proangiogenic genes,[39] resulting in a more proangiogenic environment in male hearts.

Although this study provides a framework for understanding cardiac cellular responses to a physiological stress, further work is required to demonstrate a causal relationship between specific cell types and genes and fibrosis. Moreover, limitations common to droplet-based single-cell sequencing studies, including detection of a limited number of genes and cells for each cell population, cell stress resulting from tissue dissociation, and the inability to analyze rare and difficult to isolate cell types, may have impeded the detection of important pathways for disease development. These limitations are particularly pertinent for our analysis of cardiomyocytes, where only nuclei, and, therefore, only a fraction of cardiomyocyte RNA, were analyzed. We also noted a significant correlation between cell population size and number of differentially regulated genes identified by comparing groups corresponding to AngII-treated and nontreated, and female and male. This suggests that our capacity to detect AngII-responsive and sexually dimorphic genes for smaller cell populations is limited; nevertheless, abundant cell populations are of particular interest in this initial study given their capacity to contribute to stress-induced cardiac remodeling. Last, although female and male mice were housed separately, the estrus cycles of female mice were not analyzed. This may affect the sexually dimorphic genes identified in this study.

Nevertheless, the findings of this study offer unique insights into the multifaceted mechanisms driving maladaptive remodeling of the heart, including important components of this process that are sexually dimorphic. They also highlight the utility of the single-cell transcriptomics data and the overall approach presented in this study for exploring the cardiac cellulome and its changes in the context of chronic tissue stress. Further analysis of cardiac cell networks, with integration of data from different developmental and disease states, time points, and genetic backgrounds, will advance our understanding of cardiac cellularity in health and disease.

ARTICLE INFORMATION

Correspondence

Alexander R. Pinto, BS, PhD, Baker Heart and Diabetes Institute, 75 Commercial Rd, Prahran, Victoria, Australia 3004. Email alex.pinto@baker.edu.au

Affiliations

The Jackson Laboratory, Bar Harbor, ME (M.A.M., D.A.S., G.T.S., R.P., N.A.R.). Graduate School of Biomedical Sciences, Tufts University, Boston, MA (M.A.M.). Baker Heart and Diabetes Research Institute, Melbourne, Victoria, Australia (M.S.I.D., G.E.F., T.L.G., C.D.C., A.R.P.). Centre for Cardiovascular Biology and Disease Research, La Trobe University, Melbourne, Victoria, Australia (T.L.G, C.D.C., H.D., A.V., A.R.P.).

Disclosures

None.

Supplemental Materials

Expanded Methods
Data Supplement Figures I–XXVII
Data Supplement Tables I–XII
Data Supplement Movie I
Data Supplement Excel Files I–XIII
References 40–50

REFERENCES

1. Pinto AR, Ilinykh A, Ivey MJ, Kuwabara JT, D'Antoni ML, Debuque R, Chandran A, Wang L, Arora K, Rosenthal NA, et al. Revisiting cardiac cellular composition. *Circ Res.* 2016;118:400–409. doi: 10.1161/CIRCRESAHA.115.307778

2. Blenck CL, Harvey PA, Reckelhoff JF, Leinwand LA. The importance of biological sex and estrogen in rodent models of cardiovascular health and disease. *Circ Res.* 2016;118:1294–1312. doi: 10.1161/CIRCRESAHA.116.307509

3. DeLaughter DM, Bick AG, Wakimoto H, McKean D, Gorham JM, Kathiriya IS, Hinson JT, Homsy J, Gray J, Pu W, et al. Single-cell resolution of temporal gene expression during heart development. *Dev Cell.* 2016;39:480–490. doi: 10.1016/j.devcel.2016.10.001

4. Skelly DA, Squiers GT, McLellan MA, Bolisetty MT, Robson P, Rosenthal NA, Pinto AR. Single-cell transcriptional profiling reveals cellular diversity and intercommunication in the mouse heart. *Cell Rep.* 2018;22:600–610. doi: 10.1016/j.celrep.2017.12.072

5. Farbehi N, Patrick R, Dorison A, Xaymardan M, Janbandhu V, Wystub-Lis K, Ho JW, Nordon RE, Harvey Pl. Single-cell expression profiling reveals dynamic flux of cardiac stromal, vascular and immune cells in health and injury. *Elife* 2019;8:e43882. doi:10.7554/eLife.43882.

6. Forte E, Skelly DA, Chen M, Daigle S, Morelli KA, Hon O, Philip VM, Costa MW, Rosenthal NA, Furtado MB. Dynamic interstitial cell response during myocardial infarction predicts resilience to rupture in genetically diverse mice. *Cell Rep.* 2020;30:3149–3163.e6. doi: 10.1016/j.celrep.2020.02.008

7. van den Brink SC, Sage F, Vértesy Á, Spanjaard B, Peterson-Maduro J, Baron CS, Robin C, van Oudenaarden A. Single-cell sequencing reveals dissociation-induced gene expression in tissue subpopulations. *Nat Methods.* 2017;14:935–936. doi: 10.1038/nmeth.4437

8. Ackers-Johnson M, Li PY, Holmes AP, O'Brien SM, Pavlovic D, Foo RS. A simplified, langendorff-free method for concomitant isolation of viable cardiac myocytes and nonmyocytes from the adult mouse heart. *Circ Res.* 2016;119:909–920. doi: 10.1161/CIRCRESAHA.116.309202

9. Lee DS, Gona P, Vasan RS, Larson MG, Benjamin EJ, Wang TJ, Tu JV, Levy D. Relation of disease pathogenesis and risk factors to heart failure with preserved or reduced ejection fraction: insights from the Framingham Heart Study of the National Heart, Lung, and Blood Institute. *Circulation.* 2009;119:3070–3077. doi: 10.1161/CIRCULATIONAHA.108.815944

10. Zhao S, Wu H, Xia W, Chen X, Zhu S, Zhang S, Shao Y, Ma W, Yang D, Zhang J. Periostin expression is upregulated and associated with myocardial fibrosis in human failing hearts. *J Cardiol.* 2014;63:373–378. doi: 10.1016/j.jjcc.2013.09.013

11. van Nieuwenhoven FA, Munts C, Op't Veld RC, González A, Díez J, Heymans S, Schroen B, van Bilsen M. Cartilage intermediate layer protein 1 (CILP1): a novel mediator of cardiac extracellular matrix remodelling. *Sci Rep.* 2017;7:16042. doi: 10.1038/s41598-017-16201-y

12. Tan FL, Moravec CS, Li J, Apperson-Hansen C, McCarthy PM, Young JB, Bond M. The gene expression fingerprint of human heart failure. *Proc Natl Acad Sci USA.* 2002;99:11387–11392. doi: 10.1073/pnas.162370099

13. Sergeeva IA, Christoffels VM. Regulation of expression of atrial and brain natriuretic peptide, biomarkers for heart development and disease. *Biochim Biophys Acta.* 2013;1832:2403–2413. doi: 10.1016/j.bbadis.2013.07.003

14. Fu X, Khalil H, Kanisicak O, Boyer JG, Vagnozzi RJ, Maliken BD, Sargent MA, Prasad V, Valiente-Alandi I, Blaxall BC, et al. Specialized fibroblast differentiated states underlie scar formation in the infarcted mouse heart. *J Clin Invest.* 2018;128:2127–2143. doi: 10.1172/JCI98215

15. La Manno G, Soldatov R, Zeisel A, Braun E, Hochgerner H, Petukhov V, Lidschreiber K, Kastriti ME, Lönnerberg P, Furlan A, et al. RNA velocity of single cells. *Nature.* 2018;560:494–498. doi: 10.1038/s41586-018-0414-6

16. Bergen V, Lange M, Peidli S, Wolf FA, Theis FJ. Generalizing RNA velocity to transient cell states through dynamical modeling. *BioRxiv.* 2019;820936. doi:10.1101/820936.

17. Stevens SM, von Gise A, VanDusen N, Zhou B, Pu WT. Epicardium is required for cardiac seeding by yolk sac macrophages, precursors of resident macrophages of the adult heart. *Dev Biol.* 2016;413:153–159. doi: 10.1016/j.ydbio.2016.03.014

18. Pinto AR, Godwin JW, Chandran A, Hersey L, Ilinykh A, Debuque R, Wang L, Rosenthal NA. Age-related changes in tissue macrophages precede cardiac functional impairment. *Aging (Albany NY).* 2014;6:399–413. doi: 10.18632/aging.100669

19. Fermin DR, Barac A, Lee S, Polster SP, Hannenhalli S, Bergemann TL, Grindle S, Dyke DB, Pagani F, Miller LW, et al. Sex and age dimorphism of myocardial gene expression in nonischemic human heart failure. *Circ Cardiovasc Genet.* 2008;1:117–125. doi: 10.1161/CIRCGENETICS.108.802652

20. Maric-Bilkan C, Arnold AP, Taylor DA, Dwinell M, Howlett SE, Wenger N, Reckelhoff JF, Sandberg K, Churchill G, Levin E, et al. Report of the National Heart, Lung, and Blood Institute Working Group on Sex Differences Research in Cardiovascular Disease: scientific questions and challenges. *Hypertension.* 2016;67:802–807. doi: 10.1161/HYPERTENSIONAHA.115.06967

21. Gourdie RG, Dimmeler S, Kohl P. Novel therapeutic strategies targeting fibroblasts and fibrosis in heart disease. *Nat Rev Drug Discov.* 2016;15:620–638. doi: 10.1038/nrd.2016.89

22. Gladka MM, Molenaar B, de Ruiter H, van der Elst S, Tsui H, Versteeg D, Lacraz GPA, Huibers MMH, van Oudenaarden A, van Rooij E. Single-cell sequencing of the healthy and diseased heart reveals cytoskeleton-associated protein 4 as a new modulator of fibroblasts activation. *Circulation.* 2018;138:166–180. doi: 10.1161/CIRCULATIONAHA.117.030742

23. Kretzschmar K, Post Y, Bannier-Hélaouët M, Mattiotti A, Drost J, Basak O, Li VSW, van den Born M, Gunst QD, Versteeg D, et al. Profiling proliferative cells and their progeny in damaged murine hearts. *Proc Natl Acad Sci USA.* 2018;115:E12245–E12254. doi: 10.1073/pnas.1805829115

24. Alex L, Russo I, Holoborodko V, Frangogiannis NG. Characterization of a mouse model of obesity-related fibrotic cardiomyopathy that recapitulates features of human heart failure with preserved ejection fraction. *Am J Physiol Heart Circ Physiol.* 2018;315:H934–H949. doi: 10.1152/ajpheart.00238.2018

25. Redfield MM, Jacobsen SJ, Borlaug BA, Rodeheffer RJ, Kass DA. Age- and gender-related ventricular-vascular stiffening: a community-based study.

Circulation. 2005;112:2254–2262. doi: 10.1161/CIRCULATIONAHA. 105.541078

26. Kropski JA, Blackwell TS. Endoplasmic reticulum stress in the pathogenesis of fibrotic disease. *J Clin Invest.* 2018;128:64–73. doi: 10.1172/JCI93560

27. Ayala P, Montenegro J, Vivar R, Letelier A, Urroz PA, Copaja M, Pivet D, Humeres C, Troncoso R, Vicencio JM, et al. Attenuation of endoplasmic reticulum stress using the chemical chaperone 4-phenylbutyric acid prevents cardiac fibrosis induced by isoproterenol. *Exp Mol Pathol.* 2012;92:97–104. doi: 10.1016/j.yexmp.2011.10.012

28. Groenendyk J, Lee D, Jung J, Dyck JR, Lopaschuk GD, Agellon LB, Michalak M. Inhibition of the unfolded protein response mechanism prevents cardiac fibrosis. *PLoS One.* 2016;11:e0159682. doi: 10.1371/journal. pone.0159682

29. Kassan M, Galán M, Partyka M, Saifudeen Z, Henrion D, Trebak M, Matrougui K. Endoplasmic reticulum stress is involved in cardiac damage and vascular endothelial dysfunction in hypertensive mice. *Arterioscler Thromb Vasc Biol.* 2012;32:1652–1661. doi: 10.1161/ATVBAHA.112.249318

30. Duan Q, Ni L, Wang P, Chen C, Yang L, Ma B, Gong W, Cai Z, Zou MH, Wang DW. Deregulation of XBP1 expression contributes to myocardial vascular endothelial growth factor-A expression and angiogenesis during cardiac hypertrophy in vivo. *Aging Cell.* 2016;15:625–633. doi: 10.1111/acel.12460

31. Kim RS, Hasegawa D, Goossens N, Tsuchida T, Athwal V, Sun X, Robinson CL, Bhattacharya D, Chou HI, Zhang DY, et al. The XBP1 Arm of the Unfolded Protein Response Induces Fibrogenic Activity in Hepatic Stellate Cells Through Autophagy. *Sci Rep.* 2016;6:39342. doi: 10.1038/srep39342

32. Andruska ND, Zheng X, Yang X, Mao C, Cherian MM, Mahapatra L, Helferich WG, Shapiro DJ. Estrogen receptor α inhibitor activates the unfolded protein response, blocks protein synthesis, and induces tumor regression. *Proc Natl Acad Sci USA.* 2015;112:4737–4742. doi: 10.1073/pnas. 1403685112

33. Briz V, Baudry M. Estrogen regulates protein synthesis and actin polymerization in hippocampal neurons through different molecular mechanisms. *Front Endocrinol (Lausanne).* 2014;5:22. doi: 10.3389/fendo.2014.00022

34. Noteboom WD, Gorski J. An early effect of estrogen on protein synthesis. *Proc Natl Acad Sci USA.* 1963;50:250–255. doi: 10.1073/pnas.50.2.250

35. Cuesta R, Berman AY, Alayev A, Holz MK. Estrogen receptor α promotes protein synthesis by fine-tuning the expression of the eukaryotic translation initiation factor 3 subunit f (eIF3f). *J Biol Chem.* 2019;294:2267–2278. doi: 10.1074/jbc.RA118.004383

36. Losordo DW, Isner JM. Estrogen and angiogenesis: a review. *Arterioscler Thromb Vasc Biol.* 2001;21:6–12. doi: 10.1161/01.atv.21.1.6

37. Likhite N, Yadav V, Milliman EJ, Sopariwala DH, Lorca S, Narayana NP, Sheth M, Reineke EL, Giguére V, Narkar V. Loss of estrogen-related receptor

alpha facilitates angiogenesis in endothelial cells. *Mol Cell Biol* 2019;39. doi:10.1128/mcb.00411-18.

38. Sieveking DP, Lim P, Chow RW, Dunn LL, Bao S, McGrath KC, Heather AK, Handelsman DJ, Celermajer DS, Ng MK. A sex-specific role for androgens in angiogenesis. *J Exp Med.* 2010;207:345–352. doi: 10.1084/jem. 20091924

39. Binet F, Sapieha P. ER stress and angiogenesis. *Cell Metab.* 2015;22:560–575. doi: 10.1016/j.cmet.2015.07.010

40. Pinto AR, Paolicelli R, Salimova E, Gospocic J, Slonimsky E, Bilbao-Cortes D, Godwin JW, Rosenthal NA. An abundant tissue macrophage population in the adult murine heart with a distinct alternatively-activated macrophage profile. *PLoS One.* 2012;7:e36814. doi: 10.1371/journal.pone.0036814

41. R Core Team. *R: A Language and Environment for Statistical Computing.* 2019.

42. Stuart T, Butler A, Hoffman P, Hafemeister C, Papalexi E, Mauck WM 3rd, Hao Y, Stoeckius M, Smibert P, Satija R. Comprehensive Integration of single-cell data. *Cell.* 2019;177:1888–1902.e21. doi: 10.1016/j. cell.2019.05.031

43. Linderman GC, Rachh M, Hoskins JG, Steinerberger S, Kluger Y. Fast interpolation-based t-SNE for improved visualization of single-cell RNA-seq data. *Nat Methods.* 2019;16:243–245. doi: 10.1038/s41592-018-0308-4

44. Finak G, McDavid A, Yajima M, Deng J, Gersuk V, Shalek AK, Slichter CK, Miller HW, McElrath MJ, Prlic M, et al. MAST: a flexible statistical framework for assessing transcriptional changes and characterizing heterogeneity in single-cell RNA sequencing data. *Genome Biol.* 2015;16:278. doi: 10.1186/s13059-015-0844-5

45. Soneson C, Robinson MD. Bias, robustness and scalability in single-cell differential expression analysis. *Nat Methods.* 2018;15:255–261. doi: 10.1038/nmeth.4612

46. Yu G, Wang LG, Han Y, He QY. clusterProfiler: an R package for comparing biological themes among gene clusters. *OMICS.* 2012;16:284–287. doi: 10.1089/omi.2011.0118

47. Ramilowski JA, Goldberg T, Harshbarger J, Kloppmann E, Kloppman E, Lizio M, Satagopam VP, Itoh M, Kawaji H, Carninci P, et al. A draft network of ligand-receptor-mediated multicellular signalling in human. *Nat Commun.* 2015;6:7866. doi: 10.1038/ncomms8866

48. Gu Z, Gu L, Eils R, Schlesner M, Brors B. circlize Implements and enhances circular visualization in R. *Bioinformatics.* 2014;30:2811–2812. doi: 10.1093/bioinformatics/btu393

49. Cao J, Spielmann M, Qiu X, Huang X, Ibrahim DM, Hill AJ, Zhang F, Mundlos S, Christiansen L, Steemers FJ, et al. The single-cell transcriptional landscape of mammalian organogenesis. *Nature.* 2019;566:496–502. doi: 10.1038/s41586-019-0969-x

50. Street K, Risso D, Fletcher RB, Das D, Ngai J, Yosef N, Purdom E, Dudoit S. Slingshot: cell lineage and pseudotime inference for single-cell transcriptomics. *BMC Genomics.* 2018;19:477. doi: 10.1186/s12864-018-4772-0